Asymmetry in the seasonal cycle of zonal-mean surface air temperature

Lettie A. Roach[1,2], Ian Eisenman[3], Till Wagner[4], Aaron Donohoe[5]

[1]NASA Goddard Institute for Space Studies, New York, NY, USA
[2]Center for Climate Systems Research, Columbia University, New York, NY, USA
[3]Scripps Institution of Oceanography, University of California San Diego, California, USA
[4]Atmospheric and Oceanic Sciences, University of Wisconsin Madison, Wisconsin, USA
[5]Polar Science Center, Applied Physics Laboratory, University of Washington, Seattle, WA, USA

Key Points:

- The zonal-mean seasonal cycle in surface air temperature is asymmetric
- The warming period tends to be shorter than 6 months in high latitudes and longer than 6 months in low latitudes
- The asymmetry can largely be explained by variations in top-of-atmosphere insolation, dictated by Earth's orbit

Corresponding author: L. Roach, `l.roach@columbia.edu`

Abstract

At most latitudes, the seasonal cycle of zonal-mean surface temperature is notably asymmetric: the length of the warming season is not equal to the length of the cooling season. The asymmetry varies spatially, with the cooling season being ∼40 days shorter than the warming season in the subtropics and the warming season being ∼100 days shorter than the cooling season at the poles. Furthermore, the asymmetry differs between the Northern Hemisphere and the Southern Hemisphere. Here, we show that these observed features are broadly captured in a simple model for the evolution of temperature forced by realistic insolation. The model suggests that Earth's orbital eccentricity largely determines the hemispheric contrast, and obliquity broadly dictates the meridional structure. Clouds, atmospheric heat flux convergence, and time-invariant effective surface heat capacity have minimal impacts on seasonal asymmetry. This simple, first-order picture has been absent from previous discussions of the surface temperature seasonal cycle.

Plain Language Summary

Away from the equator, most places on Earth experience a noticeable seasonal cycle in surface temperature. The seasonal cycle of temperature governs many aspects of human and ecosystem behaviour. Observations show that, at most latitudes, the length of the warming season is not equal to the length of the cooling season, i.e., the seasonal cycle is *asymmetric*. For example, at 25 °N, the average warming season is 35 days longer than the cooling season. Here, we look at how this asymmetry varies with distance from the equator. We find that the asymmetry can largely be explained as a result of variations in the amount of radiation from the sun that reaches Earth, which are determined by Earth's orbit.

1 Introduction

The seasonal cycle in surface air temperature is a fundamental feature of Earth's climate system, governing many aspects of human and ecological behaviour. Qualitatively, it is understood that the seasonal cycle in temperature is driven by the seasonal cycle in insolation, and moderated primarily by the effective heat capacity of the surface, which damps the amplitude of the seasonal cycle over the ocean more than over the land. Seasonal variations in atmospheric circulation and spatial variations in radiative feedbacks also contribute to the seasonal evolution of temperature, and may provide an

analogue to the spatial pattern of warming expected in response to anthropogenic forcing (McKinnon et al., 2013). Quantitative understanding of the seasonal cycle in surface temperature and its changes under global warming has been developed through previous analyses that focus on the phase and amplitude of the annual harmonic (Stine et al., 2009; Stine & Huybers, 2012; Dwyer et al., 2012; Donohoe & Battisti, 2013).

However, as highlighted by Donohoe, Dawson, et al. (2020), there are substantial departures in the surface air temperature from its annual harmonic that vary across the globe. These departures can be described using the difference in length between the periods of seasonal warming and cooling as a measure of asymmetry. Donohoe, Dawson, et al. (2020) propose several candidate mechanisms that may explain asymmetry in various locations, including the atmospheric versus oceanic contrast in seasonal boundary layer depth in response to solar heating, the phase differences between surface insolation and top-of-atmosphere insolation due to clouds, and the impact of seasonally-evolving atmospheric circulations such as the monsoon and stationary waves. Donohoe, Dawson, et al. (2020) stress that their analysis is exploratory, and the authors find no single mechanism that adequately explains the broad-scale features of the asymmetry.

Here, we consider asymmetry in the seasonal cycle of zonal-mean surface air temperature, and in particular we focus on latitudinal variations in asymmetry (i.e., the meridional structure of the asymmetry). We show that the broad structure of the asymmetry is consistent with idealized model results that describe the local thermodynamic response to the seasonal cycle in insolation, which features substantial departures from the annual harmonic in the high latitudes and subtropics. This model is cast as a simple ordinary differential equation forced by realistic insolation; it is adopted from Roach et al. (2022) and applied here to a different question. The predicted asymmetry is found to be mostly insensitive to the inclusion of seasonally varying clouds, atmospheric circulation, and the specification of radiative feedbacks.

2 Methods

We use the daily 2-m air temperature (T2m) from the ERA5 reanalysis (Hersbach et al., 2020) and smooth it spatially by averaging the 0.25° data onto a coarser 2° grid. Leap years are linearly interpolated to 365 days. We then take the zonal mean and compute the climatology over the first four decades of the satellite era (1979–2018). Even

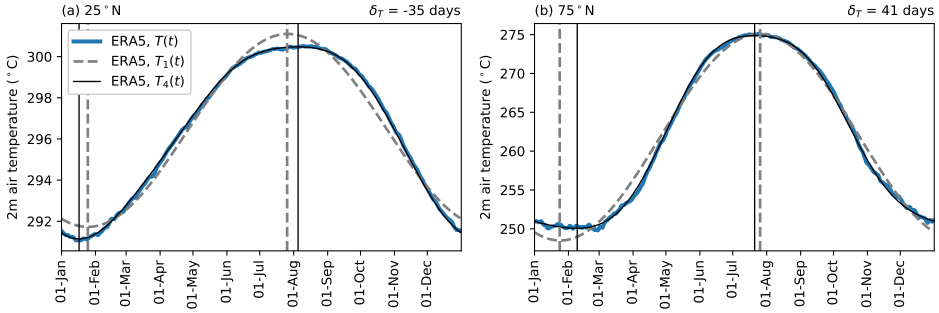

Figure 1. Example seasonal cycles of T2m at (a) 25°N and (b) 75°N from ERA5, with data after spatial and temporal averaging shown in black, the annual harmonic in grey dashed, and the Fourier fit with four harmonics in blue. The times of maximum and minimum are indicated by vertical lines. The value of δ_T is marked in the upper right.

after this spatial coarsening and temporal and spatial averaging, the seasonal cycle of T2m is visibly not smooth, and the computation of the timing of the maximum and the minimum of the seasonal cycle is sensitive to "noise" from internal variability. To further remove this noise, we fit a Fourier series with four harmonics to the zonal-mean climatological seasonal cycle of T2m at each latitude, θ. Specifically, we write

$$T_4(t,\theta) = \tfrac{1}{2}\xi_0(\theta) + \sum_{n=1}^{4} \xi_n(\theta)\cos\left[2\pi n t - \phi_n(\theta)\right], \tag{1}$$

where $\xi_n(\theta)$ and $\phi_n(\theta)$ are the Fourier coefficients (results are similar when using 2-10 harmonics, as shown in Fig. S1). Fig. 1 shows zonal-mean seasonal cycles at specific example latitudes from ERA5 alongside a Fourier series with one harmonic (T_1, which contains only the annual harmonic and is symmetric) and a Fourier series with four harmonics, T_4.

We then compute the days of maximum and minimum temperature from the Fourier fit with four harmonics, T_4 (vertical solid black lines in Fig. 1). We define the length of the warming season as the duration from the minimum to the maximum of T_4. The length of the cooling season is similarly the duration from maximum to minimum, or equivalently 365 days minus the length of the warming season. As a measure of asymmetry, we define δ_T as the difference between the lengths of the warming and cooling season (as in Roach et al. (2022)). Positive δ_T values represent a shorter warming season than cooling season and negative values represent a shorter cooling season than warming season. For example, at 75°N, the date of minimum T_4 is delayed relative to its annual harmonic

counterpart, whereas the date of maximum T_4 precedes maximum T_1 (see vertical black and grey-dashed lines in Fig. 1b), with a warming season length of 162 days and a cooling season length of 203 days. This indicates a shorter warming season and positive δ_T, with $\delta_T = 41$ days.

Globally, results are similar using the JRA55 reanalysis (Japan Meteorological Agency, 2013) in place of ERA5, although there are some deviations over the Antarctic continent (Fig. S2).

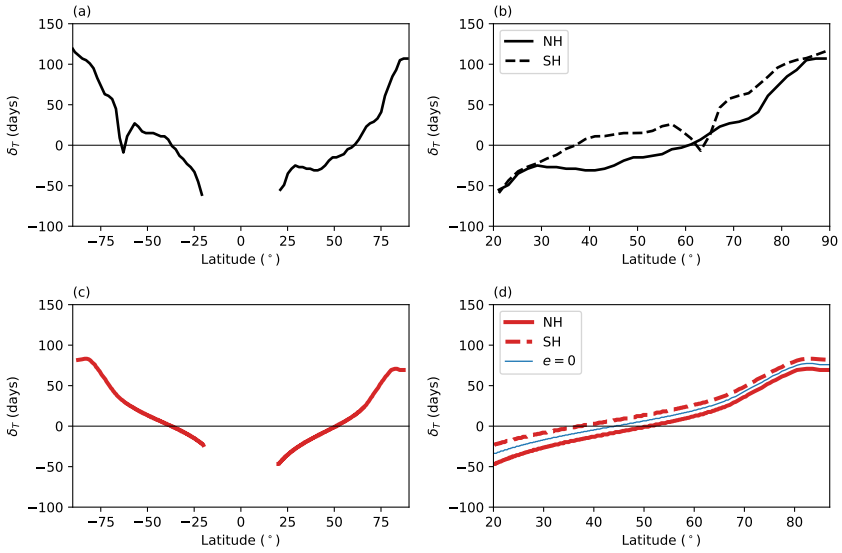

Figure 2. Meridional structure of asymmetry (δ_T). (a) Asymmetry computed from ERA5 output; (b) as in panel (a) but with values for the Southern Hemisphere plotted at their equivalent Northern latitudes. (c-d) as in panels (a-b) but for the solution to Eq. 2, forced by present-day top-of-atmosphere (TOA) insolation. The thin blue line in panel (d) shows δ_T from the solution to Eq. 2 with TOA insolation corresponding to zero orbital eccentricity.

3 Results

To investigate large-scale drivers of asymmetry in the seasonal cycle of T2m, we first consider the broad-scale structure in the zonal-mean seasonal cycle. Zonal variations in observed asymmetry are shown by Donohoe, Dawson, et al. (2020), who emphasize the land-ocean contrast in δ_T, which is readily apparent in the maps. Averaging T2m into the zonal mean reveals a striking meridional structure in observed δ_T (Fig. 2a), which is the focus of the present study. Values of δ_T exceed 100 days near the poles, cross zero

in the mid-latitudes, and reach -50 days in the tropics. Equatorward of 20°, we do not compute δ_T because there are typically two local maxima and minima in T2m each year. δ_T crosses zero ($\delta_T = 0$ days represents symmetry in the seasonal cycle of T2m) at 61° in the Northern Hemisphere and 37° in the Southern Hemisphere. There is a deviation from this overall pattern in the Southern Hemisphere, with δ_T crossing zero again at 64°S. The hemispheric differences are highlighted in Fig. 2b by plotting values for the Southern Hemisphere at their equivalent Northern latitudes. Values in the two hemispheres are offset by around 20 days on average, with higher values in the Southern Hemisphere (Fig. 2b).

We can gain understanding of the mechanisms controlling the meridional structure of δ_T using the framework of an idealized climate model. Roach et al. (2022) show that a substantial asymmetry in the seasonal cycle of temperature ($\delta_T \approx 1$ month) at high latitudes is obtained when solving a simple ordinary differential equation (ODE) in which seasonal variations in insolation are balanced locally by heating and radiative feedbacks. Hence we adopt Eq. 7 from Roach et al. (2022):

$$c_w \frac{dT(t,\theta)}{dt} = a(\theta)S(t,\theta) - [A + BT(t,\theta)]\,, \tag{2}$$

where c_w is the heat capacity of the ocean mixed layer, chosen to approximate a 75 m mixed layer depth, T is the surface temperature departure from some reference value, and outgoing longwave radiation is approximated as $A + B\,T$ (Budyko, 1969; Koll & Cronin, 2018) with A and B constants. Top-of-atmosphere (TOA) insolation S is computed using present-day orbital parameters following Huybers and Eisenman (2006) and Rose (2018) and is scaled by planetary coalbedo a, where $a = a_0 - a_2 \sin^2\theta$ with a_0, and a_2 constants. Initial parameter values are shown in Table S1. Note that asymmetry in temperature is always insensitive to A. We solve Eq. 2 numerically, using 100 simulation years, discretized with 1000 timesteps per year and 800 gridboxes in one spatial dimension running from pole to pole (0.1° resolution at the equator to 2° at the poles). Importantly, the equation neglects many factors including seasonal variations in atmospheric heat transport, cloud albedo, and spatial variations in radiative feedbacks—we return to the impact of these neglected processes later.

The asymmetry in the seasonal cycle in temperature, δ_T, simulated using Eq. 2 is shown in Fig. 2c. This captures the broad-scale features shown in observations. In the simulations, δ_T decreases from 80 days near the poles to -50 days in the tropics. It crosses

zero at 51° in the Northern Hemisphere and 37° in the Southern Hemisphere, similar to the observations. Values in the two hemispheres are offset by around 17 days on average, with higher values in the Southern Hemisphere (Fig. 2d), as compared with 20 days in observations (Fig. 2b). Thus, the simple ODE quantitatively reproduces two essential features of the observed spatial structure of δ_T: (i) more positive values in the Southern Hemisphere as compared to the same latitudes in the Northern Hemisphere, and (ii) positive values in the polar regions and negative values in the subtropics.

We first consider the hemispheric difference in δ_T. The eccentricity of Earth's orbit is key to the hemispheric difference in simulated temperature asymmetry. We re-compute TOA insolation using the code from Rose (2018) with eccentricity set to $e = 0$ rather than its present-day value of $e = 0.017$. In this case, solving Eq. 2 yields identical values for both hemispheres (blue line in Fig. 2d).

Secondly, we consider the meridional structure of δ_T, i.e., the general pattern of increasing δ_T from negative values in the tropics to positive values near the poles, which is retained after setting eccentricity to zero. This general pattern results from the obliquity (or tilt) of Earth's rotation relative to the plane of its orbit, which causes the seasonal cycle to depart from its annual harmonic in ways that are qualitatively different at high and low latitudes (left panels of Fig. 3). At high latitudes, the insolation minimum is prolonged and the insolation maximum is larger and more concentrated than its annual harmonic (Fig. 3a). In contrast, at subtropical latitudes, the insolation minimum is more peaked while the insolation maximum is more prolonged than the corresponding annual harmonic (Fig. 3c).

To understand how the departures in insolation from the annual harmonic impact δ_T, we further simplify Eq. 2 by omitting radiative feedbacks, i.e. setting $B = 0$. As discussed in Roach et al. (2022) (Text S1), the dominant balance in the ODE for annual forcing is between insolation and heating. Decomposing the insolation forcing as $S = \overline{S} + S'(t)$, where $\overline{S}$ is the annual mean and $S'(t) \equiv S - \overline{S}$ is the seasonally-varying departure, and similarly for temperature, we obtain:

$$\frac{dT'(t,\theta)}{dt} = -\frac{T'(t,\theta)B}{c_w} + \frac{a(\theta)\,S'(t,\theta)}{c_w}. \tag{3}$$

In the regime where $\frac{dT'}{dt} \gg \frac{T'B}{c_w}$, this becomes

$$\frac{dT'(t,\theta)}{dt} \approx \frac{a(\theta)\,S'(t,\theta),}{c_w}, \tag{4}$$

which is Eq. S4 in Roach et al. (2022). In this case, the temperature is in quadrature with the forcing. Therefore, having a narrow summer insolation peak with $S > \overline{S}$ and a wider winter insolation trough with $S < \overline{S}$, as occurs in high latitudes, leads to a brief summer warming period and a longer winter cooling period, as discussed equivalently for sea ice in Roach et al. (2022). Conversely, having a wide summer insolation peak with $S > \overline{S}$ and a narrow winter insolation trough with $S < \overline{S}$, as occurs in low latitudes, leads to a long summer warming period and a brief winter cooling period (Fig. 3).

The impact of obliquity on δ_T can be recovered when using only the first two harmonics of TOA insolation,

$$S_2(t,\theta) = \tfrac{1}{2}\xi_0(\theta) + \sum_{n=1}^{2} \xi_n(\theta)\cos\left[2\pi n t - \phi_n(\theta)\right], \tag{5}$$

to force Eq. 2 (Fig. S3). The solution for temperature in Eq. 3 forced by two harmonics in insolation (Eq. 4) is the superposition of two temperature harmonics in quadrature phase with the insolation harmonics,

$$T_2(t,\theta) \approx \frac{a(\theta)}{2\pi c_w} \sum_{n=1}^{2} n\xi_n(\theta)\sin\left[2\pi n t - \phi_n(\theta)\right]. \tag{6}$$

Thus, the temperature response to obliquity is essentially a consequence of the relative phasing of the annual and semi-annual components of insolation, which vary by latitude and sum to make the seasonal peaks and troughs of insolation broader and narrower than those of the annual harmonic alone.

While the broad-scale features of δ_T can be obtained considering only the remarkably simple Eq. 2, we also consider some modifications to this expression. Simulated amplitudes for T can be brought into agreement with observations by tuning c_w for each latitude. Changes to c_w corresponding to ocean mixed layer depths between 10 and 200 m do not substantially alter δ_T (Fig. S4). As c_w increases, the system remains in the regime where $\frac{dT'}{dt} \gg \frac{T'B}{c_w}$, so the temperature response remains in quadrature with the forcing. Minor differences in asymmetry arise when c_w tends towards the heat capacity of land, c_l (we use $c_l = 0.336$ W yr m^{-2} K^{-1} following North and Coakley (1979)), for example over the fully-land-covered latitudes of the Antarctic continent (Fig. S5).

Eq. 2 is conceptualized as a description of the surface energy balance with a parameterized radiative feedback to space forced by downwelling solar radiation at the surface. The modification of TOA insolation by co-albedo a in Eq. 2 accounts for the reflection of insolation by clouds, but it assumes that cloud reflection is seasonally invari-

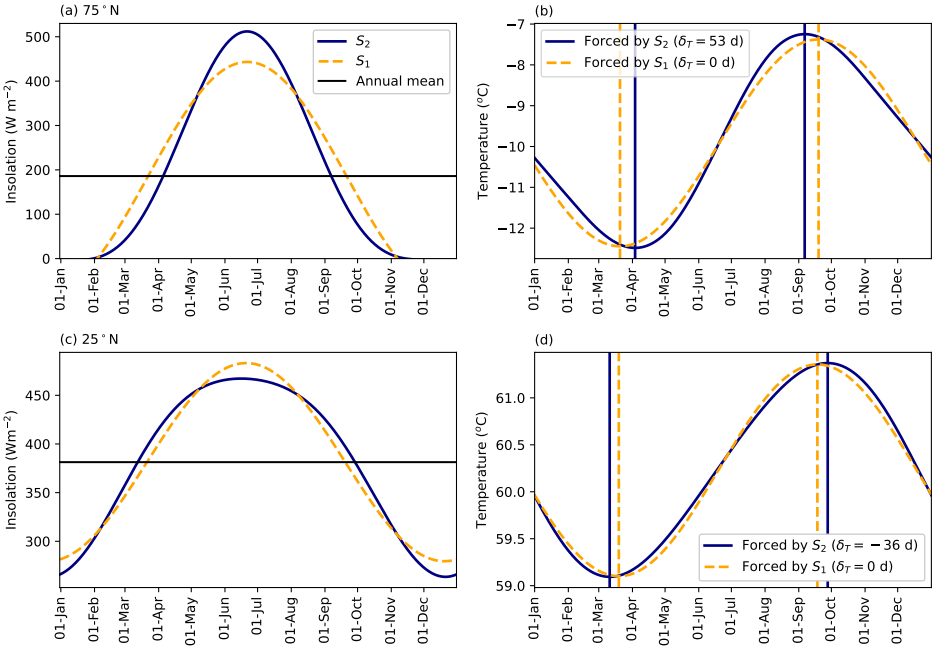

Figure 3. Left panels: Fourier series of the TOA insolation truncated at $N = 1$ and $N = 2$ at (a) 75°N and (c) 25°N. Right panels: the solution $T(t)$ to Eq. 2 when forced by the corresponding insolation as marked in the left panels, for (b) 75°N and (d) 25°N.

ant. We assess how seasonally-evolving cloud cover might impact δ_T by forcing Eq. 2 instead with surface zonal-mean downwelling shortwave radiation from CERES (Doelling et al., 2013, 2016), i.e., including the net shortwave effect of clouds instead of using TOA insolation. This has a relatively minor effect, although it amplifies asymmetry near the poles (Fig. S6). Note that the higher values of δ_T here are somewhat closer to those seen in observations. We also modify Eq. 2 to account in a simple way for atmospheric heat flux convergence based on ERA5 data (Donohoe, Armour, et al., 2020). The impact on δ_T is similar to or smaller in magnitude than switching from TOA to surface shortwave; note that it adds more meridional structure to the smooth curve that is obtained from Eq. 2 alone (Fig. S7).

As demonstrated by Donohoe, Dawson, et al. (2020) (see also Fig. S8a), there are substantial zonal variations in asymmetry across the globe. To examine the role of zonal variations in cloud cover, we force Eq. 2 with surface downwelling shortwave radiation from CERES across longitudes λ and solve for $T(\theta, \lambda)$. The impacts are minor in most regions, with the exception of the Indian subcontinent and the North Pacific (Fig. S8b,f).

The seasonal cycle of the fraction of shortwave absorbed by clouds over these two regions is nearly opposite. Over the Indian subcontinent, there are more clouds in the summer/early fall season due to summer monsoon activity, whereas in the North Pacific region, there are more clouds in the winter/spring season due to storm activity. Our simple model accounting for the impact of clouds cannot explain other zonally-varying departures from the overall pattern expected based on insolation, including southeast of the South American continent and south of New Zealand.

4 Conclusions

The seasonal cycle of surface temperature has a large amplitude outside the tropics. Furthermore, the climatological seasonal evolution of temperature can serve as a test of our understanding of the underlying physics of the climate system, as it represents a well-observed response to a large change in solar forcing. The seasonal cycle is shaped by a variety of factors, including the tilt of the Earth's axis, Earth's orbital eccentricity, global atmospheric circulation patterns, and land surface characteristics. A number of previous studies have analyzed the seasonal cycle using the amplitude and phase of the annual harmonic, which is symmetric. However, at most latitudes, the seasonal cycle of temperature is strikingly asymmetric, deviating from symmetry by around -40 days in the subtropics and 100 days at the poles. Donohoe, Dawson, et al. (2020) suggested a number of possible mechanisms that could contribute to this asymmetry, but nothing that could describe the broad-scale features.

Here, adopting the approach of Roach et al. (2022), we suggest that the broad meridional structure of asymmetry in the zonal-mean seasonal cycle of surface temperature results directly from variations in top-of-atmosphere insolation. The eccentricity of Earth's orbit generates the difference in asymmetry between the two hemispheres. The obliquity, or axial tilt, of the Earth generates much of the variation in asymmetry from the tropics to the poles, and it dictates the latitude where the seasonal cycle is symmetric. In the reanalysis products analyzed, values of asymmetry are on average 20 days higher in the Southern Hemisphere than the Northern Hemisphere (averaging over latitudes polewards of 20°). Using a simple idealized model of the evolution of surface temperature forced by realistic insolation, we reproduce both effects, with an average hemispheric difference of 17 days. Moreover, both effects can be captured using a simplified variant of the model forced by only two harmonics of the insolation.

We find that the asymmetry of the seasonal cycle of zonal-mean surface temperature arises primarily due to the direct thermodynamic response to insolation forcing. Our results suggest that clouds and atmospheric heat flux convergence do not play a substantial role in modulating the zonal-mean structure of asymmetry, although clouds impact temperature asymmetry in certain regions, specifically the North Pacific and the Indian subcontinent. Seasonal asymmetry may also be influenced by factors not considered here, including seasonal changes in surface effective heat capacity. The simple first-order picture presented here has been absent from previous discussions of the seasonal cycle of surface temperature.

5 Open Research

The ERA5 reanalysis (Hersbach et al., 2020) is available from ECMWF (`https://www.ecmwf.int/en/forecasts/datasets/reanalysis-datasets/era5` [Date Accessed: 03-2022]). CERES SYN data (Doelling et al., 2013, 2016) were obtained from the NASA Langley Research Center Atmospheric Science Data Center (`https://ceres-tool.larc.nasa.gov/ord-tool/jsp/SYN1degEd41Selection.jsp` [Date Accessed: 03-2022]). The JRA55 reanalysis (Japan Meteorological Agency, 2013) is available from `https://rda.ucar.edu/datasets/ds628.0/` [Date Accessed: 03-2022]. Model output is currently available at `https://drive.google.com/file/d/1DccQX6rHz7e-YQH8D2adCdsA5vTv18ce/view?usp=share_link` and will be published on Zenodo by the time of publication.

Acknowledgments

LR was supported by the National Oceanic and Atmospheric Administration (NOAA) Climate and Global Change Postdoctoral Fellowship Program, which is administered by UCAR's Cooperative Programs for the Advancement of Earth System Science (CPAESS) under award NA18NWS4620043B and the NASA Modeling Analysis and Prediction program. This work was also supported by National Science Foundation (NSF) grant 2048590. The authors would like to acknowledge computing and data storage resources, including the Cheyenne supercomputer (`https://doi.org/10.5065/D6RX99HX`) provided by the Computational and Information Systems Laboratory (CISL) at NCAR. We also thank the two anonymous reviewers, whose comments improved the paper.

References

Budyko, M. I. (1969, October). The effect of solar radiation variations on the climate of the Earth. *Tellus*, *21*(5), 611–619. Retrieved from http://doi.wiley.com/10.2307/1930283 (ISBN: 00129658) doi: 10.1111/j.2153-3490.1969.tb00466.x

Doelling, D. R., Loeb, N. G., Keyes, D. F., Nordeen, M. L., Morstad, D., Nguyen, C., ... Sun, M. (2013, June). Geostationary Enhanced Temporal Interpolation for CERES Flux Products. *Journal of Atmospheric and Oceanic Technology*, *30*(6), 1072–1090. Retrieved 2023-01-26, from https://journals.ametsoc.org/view/journals/atot/30/6/jtech-d-12-00136_1.xml (Publisher: American Meteorological Society Section: Journal of Atmospheric and Oceanic Technology) doi: 10.1175/JTECH-D-12-00136.1

Doelling, D. R., Sun, M., Nguyen, L. T., Nordeen, M. L., Haney, C. O., Keyes, D. F., & Mlynczak, P. E. (2016, March). Advances in Geostationary-Derived Longwave Fluxes for the CERES Synoptic (SYN1deg) Product. *Journal of Atmospheric and Oceanic Technology*, *33*(3), 503–521. Retrieved 2023-01-26, from https://journals.ametsoc.org/view/journals/atot/33/3/jtech-d-15-0147_1.xml (Publisher: American Meteorological Society Section: Journal of Atmospheric and Oceanic Technology) doi: 10.1175/JTECH-D-15-0147.1

Donohoe, A., Armour, K. C., Roe, G. H., Battisti, D. S., & Hahn, L. (2020, April). The Partitioning of Meridional Heat Transport from the Last Glacial Maximum to CO2 Quadrupling in Coupled Climate Models. *Journal of Climate*, *33*(10), 4141–4165. Retrieved 2023-01-30, from https://journals.ametsoc.org/view/journals/clim/33/10/jcli-d-19-0797.1.xml (Publisher: American Meteorological Society Section: Journal of Climate) doi: 10.1175/JCLI-D-19-0797.1

Donohoe, A., & Battisti, D. S. (2013). The seasonal cycle of atmospheric heating and temperature. *Journal of Climate*, *26*(14), 4962–4980. doi: 10.1175/JCLI-D-12-00713.1

Donohoe, A., Dawson, E., McMurdie, L., Battisti, D. S., & Rhines, A. (2020). Seasonal Asymmetries in the Lag between Insolation and Surface Temperature. *Journal of Climate*, *33*(10), 3921–3945. doi: 10.1175/jcli-d-19-0329.1

Dwyer, J. G., Biasutti, M., & Sobel, A. H. (2012). Projected changes in the seasonal cycle of surface temperature. *Journal of Climate*, *25*(18), 6359–6374. doi: 10.1175/JCLI-D-11-00741.1

Hersbach, H., Bell, B., Berrisford, P., Hirahara, S., Horányi, A., Muñoz-Sabater, J., ... Thépaut, J. (2020, July). The ERA5 global reanalysis. *Quarterly Journal of the Royal Meteorological Society*, *146*(730), 1999–2049. doi: 10.1002/qj.3803

Huybers, P., & Eisenman, I. (2006). *Integrated Summer Insolation Calculations.* IGBP PAGES/World Data Center for Paleoclimatology. (Place: NOAA/NCDC Paleoclimatology Program, Boulder CO, USA.)

Japan Meteorological Agency. (2013). *JRA-55: Japanese 55-year Reanalysis, Daily 3-Hourly and 6-Hourly Data.* Retrieved from `http://doi.org/10.5065/D6HH6H41` (Medium: Archive at the National Center for Atmospheric Research, Boulder, CO, United States) doi: 10.5065/D6HH6H41

Koll, D. D. B., & Cronin, T. W. (2018, October). Earth's outgoing longwave radiation linear due to H2O greenhouse effect. *Proceedings of the National Academy of Sciences*, *115*(41), 10293–10298. Retrieved 2023-01-24, from `https://www.pnas.org/doi/10.1073/pnas.1809868115` (Publisher: Proceedings of the National Academy of Sciences) doi: 10.1073/pnas.1809868115

McKinnon, K. A., Stine, A. R., & Huybers, P. (2013, October). The spatial structure of the annual cycle in surface temperature: Amplitude, phase, and lagrangian history. *Journal of Climate*, *26*(20), 7852–7862. Retrieved from `https://journals.ametsoc.org/jcli/article/26/20/7852/33736/The-Spatial-Structure-of-the-Annual-Cycle-in` doi: 10.1175/JCLI-D-13-00021.1

North, G. R., & Coakley, J. A. (1979). Differences between Seasonal and Mean Annual Energy Balance Model Calculations of Climate and Climate Sensitivity. *Journal of the Atmospheric Sciences*, *36*, 1189–1204. Retrieved from `http://dx.doi.org/10.1175/1520-0469(1979)036%3C1189:DBSAMA%3E2.0.CO;2%5Cnhttp://adsabs.harvard.edu/abs/1979JAtS...36.1189N` (ISBN: 0022-4928) doi: 10.1175/1520-0469(1979)036⟨1189:DBSAMA⟩2.0.CO;2

Roach, L. A., Eisenman, I., Wagner, T. J. W., Blanchard-Wrigglesworth, E., & Bitz, C. M. (2022, April). Asymmetry in the seasonal cycle of Antarc-

tic sea ice driven by insolation. *Nature Geoscience*, *15*(4), 277–281. Retrieved from https://www.nature.com/articles/s41561-022-00913-6 doi: 10.1038/s41561-022-00913-6

Rose, B. E. j. (2018, April). CLIMLAB: a Python toolkit for interactive, process-oriented climate modeling. *Journal of Open Source Software*, *3*(24), 659. Retrieved 2023-02-02, from https://joss.theoj.org/papers/10.21105/joss.00659 doi: 10.21105/joss.00659

Stine, A. R., & Huybers, P. (2012, November). Changes in the Seasonal Cycle of Temperature and Atmospheric Circulation. *Journal of Climate*, *25*(21), 7362–7380. Retrieved 2022-11-07, from https://journals.ametsoc.org/doi/10.1175/JCLI-D-11-00470.1 doi: 10.1175/JCLI-D-11-00470.1

Stine, A. R., Huybers, P., & Fung, I. Y. (2009). Changes in the phase of the annual cycle of surface temperature. *Nature*, *457*(7228), 435–440. (Publisher: Nature Publishing Group) doi: 10.1038/nature07675